Mine Water Environ (2017) 36:283–298
DOI 10.1007/s10230-017-0442-8

TECHNICAL ARTICLE

Combined Use of Geostatistics and Multi-Criteria Decision Analysis to Determine New Pumping Well Locations in the Gol-Gohar Open Pit Mine, Iran

Amin Assari[1] · **Zargham Mohammadi**[1]

Received: 12 September 2015 / Accepted: 16 February 2017 / Published online: 18 March 2017

Abstract Groundwater seepage into open pit mines must be controlled carefully. Slope instability, dewatering of blast holes, and mining operations below the groundwater table are important issues caused by groundwater seepage into the Gol-Gohar open pit mine, Iran. There are several methods to overcome these problems, such as construction of cut-off walls, ditches and sumps, horizontal drains, and pumping wells. Drilling of a new pumping well has several difficulties in which the determination of its location is a major issue. In this study, a stochastic simulation approach called simulated annealing was used to determine the best possible locations for new pumping wells. Three major groundwater variables, including the groundwater level, electrical conductivity, and transmissivity were selected for the geostatistical study. The results of simulations showed reliable correlation (Pearson) between the variables. Comparison of the variograms at different depths of the Gol-Gohar pit mine revealed that the effect of faults intensified with increasing depth. The best potential locations for drilling of new pumping wells were identified by the use of multi-criteria decision analysis performed on the simulation results. This method can be used in other regions with similar hydrogeological settings.

Keywords Stochastic simulation · MCDA · Dewatering · Gol-Gohar open pit mine · Iran

✉ Zargham Mohammadi
zmohammadi@shirazu.ac.ir

Amin Assari
a.assari@goharzamin.com

[1] Department of Earth Science, Faculty of Science, Shiraz University, Shiraz, Iran

Introduction

One of the most important problems at mine sites, especially in open pit mines, is groundwater and its impact on mining operations. Mine development and subsequent activities disturb the normal groundwater hydraulic gradient. The situation becomes more complicated over time when the groundwater hydraulic gradient increases. In some situations, this dilemma may exacerbate and could result in significant loss of life and property. For example, groundwater bursting, which may be instantaneous or retarded, can cause several problems during mining operations (Li et al. 2011; Wu et al. 2004). Groundwater inflow into the pits may occur via preferential pathways induced by faults. Movement of groundwater along faults is easier than in the rock matrix and transmissivity along these routes can vary by several orders of magnitude. On the other hand, faults may form a barrier lateral to flow direction depending on whether the fault zones are more or less permeable than the adjoining aquifers (Bredehoeft et al. 1992). Thus, in order to describe and model the spatial distribution of groundwater, it is crucial to study the location and mechanism of faulting, especially in tectonically active regions (e.g. Forster and Evans 1991; López and Smith 1995; Smerdon and Turnadge 2015).

There are several ways to control groundwater invasion along faults in open pit mines, such as the construction of cut-off walls, underground galleries, ditches and trenches, horizontal drains and sumps, and pumping wells (e.g. Golestanifar and Ahangari 2012; Morton and Van Mekerk 1993). To design a dewatering system, several important things must be considered, including the hydrogeological conditions, volume of water to be removed, transmissivity and storage coefficient of aquifer, and depth and thickness of the aquifer (Morton

and Van Mekerk 1993). Pumping from well points is an effective approach, but it requires deciding where to locate the wells. Depending on the objectives of the study, there is usually a tendency to locate the pumping wells in areas with high permeability. This requires a clear and comprehensive knowledge of the hydrogeological characteristics of the aquifer. Although this is unattainable in reality, it can be performed using several methods. Yin and Brook (1992) studied topographic and fracture trace data from 29 wells to locate sites for high-yield wells. Huang and Mayer (1997) used an optimization formulation and a genetic algorithm to determine optimal pumping rates and the discrete spacing of well locations. Stevick et al. (2005) used a probabilistic approach and simulated thousands of Monte Carlo realizations to locate new production wells. Geoelectrical methods (e.g. Chandra et al. 2008; Niwas et al. 2011) and inverse modelling have been used to estimate hydraulic properties from measured variables such as hydraulic head, concentration data, etc. (e.g. Hill and Tiedeman 2006; Sun 1994; Worthington 2009).

Geostatistics is one of the best methods for evaluation and estimation of hydraulic parameters and is regarded as a promising method for characterizing heterogeneous media. It has the advantage that it can be fully conditioned on all the available local information, even on indirect data such as hydraulic heads (De Marsily et al. 1998). This approach has widely been used in hydrogeological studies for estimation and simulation of hydraulic properties, e.g. transmissivity and hydraulic conductivity. Huysmans and Dassargues (2009) applied multiple-point geostatistics and variogram-based geostatistical methods to simulate permeability to determine the impact of complex geological heterogeneity on groundwater flow. Other studies include Jang and Liu (2004), Nowak and Cirpka (2006), Patriarche et al. (2005), and Soltani-Mohammadi and Hezarkhani (2013).

The Gol-Gohar mine is located in the south of Iran and is a part of the Central Iran structural zone. Groundwater seepage into the pit mine has created several problems, including slope instability, dewatering of blast holes, and mining operations below the groundwater table. In this study, three main parameters, including groundwater level (GWL), electrical conductivity (EC), and transmissivity were used to assess and evaluate the hydrogeological setting of the pit mine and locate the most permeable zones for drilling new pumping wells. Most of the values for these parameters were simulated over the study area by the use of the annealing method. A multi-criteria decision analysis was then applied to the simulation results to identify the best places for drilling new wells.

Study Area

The Gol-Gohar open pit mine is situated 45 km southwest of Sirjan City, Kerman Province, Iran and located between 55° 15′40″, 55° 22′33″, longitudes and 29° 3′10″, 29° 7′4″ latitudes. The main geographical features are the Chah-Barreh and Einolbaghar Mountains in the southern parts of the study area (Fig. 1). These mountains have a NW-SE trend similar to the Sanandaj-Sirjan structural zone. There are five open pits; pit 1 has the largest area (1.48 km^2) and a depth of 120–130 m (Figs. 2, 3). This study focused on a hydrogeological and hydrochemical assessment of this pit.

Geological Setting

Geologically, the study area is part of the Sanandaj-Sirjan metamorphic zone, one of the five main structural zones in Iran (Alavi 1994). Metamorphic rocks of Palaeozoic age outcrop in the study area and consist of five units: (1) serpentinized ultramafic rocks and metamorphic gabbros; (2) dolomitized marbles to calcic marbles; (3) micaschist, gneiss and amphibolites; (4) gneiss; and (5) calcic marbles, gneiss, micaceous schist, schist, and quartzites. The main part of the study area is underlain by thick alluvial deposits with a thickness of up to 205 m (Figs. 2, 3). These deposits consist of detrital sediments, which are composed of an alternating sequence of conglomerates, sandstone, marl, and gypsiferous clays with thin interlayers of limestone.

The faults in the study area can be divided into regional and local faults. Many of the regional faults are reverse and thrust types. Local faults (Fig. 2) are divided into two groups, according to their age: (1) Pliocene-Quaternary faults and; (2) older faults.

Hydrogeology

Several hydrogeological and geophysical studies have been conducted in the study area. Previous studies showed that there are two main aquifers, which can be distinguished by criteria such as hydrochemical characteristics, hydraulic head, and lithology. Table 1 shows the general characteristics of these aquifers. Based on hydrochemical criteria, the lower hard rock aquifer has a higher EC (with a mean of 24.1 mS/cm); the upper aquifer, which is composed of alluvial deposits, has a lower EC (with a mean of 10.8 mS/cm). The lower aquifer also has higher transmissivity values (averaging 299.4 m^2/d) compared to the upper aquifer (averaging 188.9 m^2/d). The increased density of fracture zones with depth is likely the main reason for such variations in average transmissivity. Another important hydrogeologic parameter is the groundwater level, which is also different for the lower and upper aquifers. Previous studies showed that the two aquifers are hydraulically connected

and that no impermeable layer exists between them (Kusha Maadan Consulting Engineers 2006). However, the hydraulic connection seems to be limited because of the difference in GWL. The average groundwater level in the upper aquifer is 1685.11 m above sea level (asl), whereas it is 1681.87 m asl in the lower aquifer.

Figure 4 illustrates the vertical hydraulic gradients calculated from the average groundwater levels in the piezometers installed at various depths over the study area. All piezometers located within the pit showed large vertical hydraulic gradients, ranging from 0.046 to 0.730. The high values of the vertical hydraulic gradient are mainly attributed to the effect of pumping from the wells within the pit. Because of the high transmissivity of the lower aquifer, it is assumed that it mainly contributes to the discharge from the pumping wells. This causes the lower aquifer to have lower groundwater levels than the upper aquifer. The considerable difference in the water levels of the lower and upper aquifers would suggest that they are not hydraulically connected, but it is also possible that other factors contribute

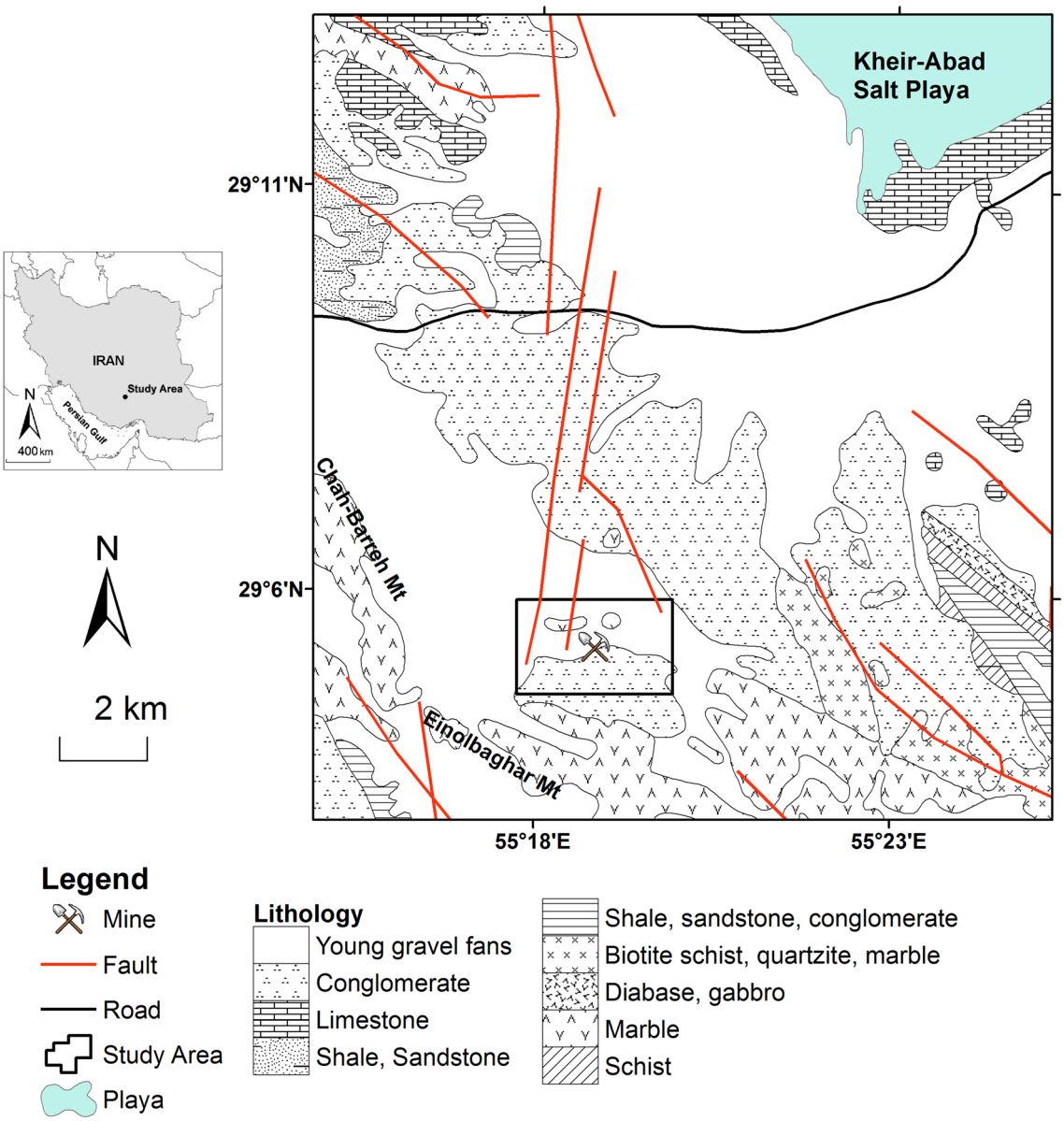

Fig. 1 The study area and the location of some major geological structures. Alluvial deposits cover the main part of the study area, while metamorphic rock outcrops in some areas. The Kheir-Abad salt playa is located in the northeastern part of the study area

to the contrasting difference between the water levels in the two aquifers, e.g. differences in their storage coefficients and recharge rates.

The hard rock aquifer is mainly composed of metamorphic rocks such as magnetite, mica schist and amphibolite (Fig. 3), whereas the alluvial aquifer is composed of young gravel fans and conglomerate (Fig. 1). The general flow direction of groundwater in both aquifers is from the NE towards the SW (Kusha Maadan Consulting Engineers 2007). However, the development of pit 1 has disturbed the general groundwater flow direction, with flow currently concentrated towards the centre of the pit. The hydraulic gradient of the alluvial aquifer has a wide range (from 0.00008 to 0.1) over the study area. The highest hydraulic gradient exists at the NE and E portion of the pit (about 0.1) and is due to dewatering. The hydraulic gradient in the lower aquifer also ranges widely, from 0.00005 to 0.35; the maximum value occurs in the southeastern portion of the pit.

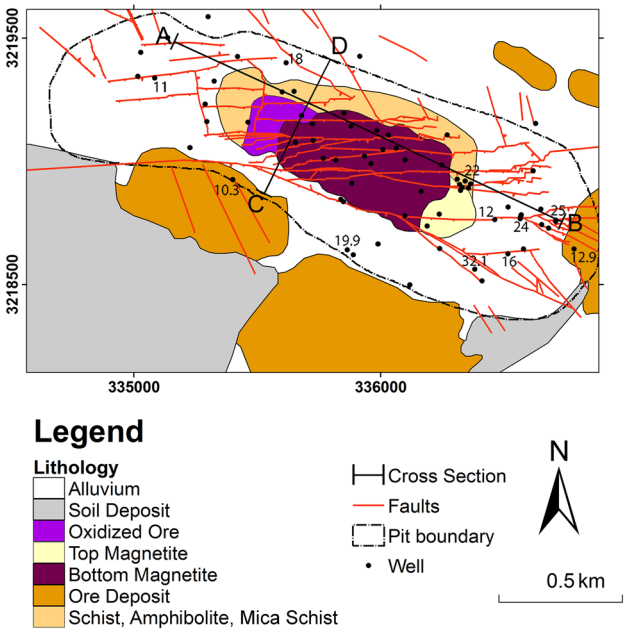

Fig. 2 Location of the mine pit and the local faults. The AB and CD cross sections are presented in Fig. 3. The faults are oriented in a NW-SE direction. The *numbers* next to the well points represent the discharge rate (L/s) from the pumping-wells. *Other point symbols* represent the observation wells and piezometers (Datum: WGS_1984 UTM Zone 40 N)

Method of Study

In this section, we present the reasons for using transmissivity, EC, and groundwater level to locate suitable places for new wells. This is followed by introducing the number of data points, frequency of sampling, and methods used for measuring these properties. After that, the theory of simulated annealing and multi-criteria decision analysis are outlined.

Hydrogeological and Hydrochemical Parameters

Three important variables, groundwater level, EC, and transmissivity, were considered and then examined using statistical and geostatistical approaches to characterize the most favourable places for drilling new pumping wells. Transmissivity is a major hydrogeological property of every water-bearing formation and controls the capability of aquifers to transmit water. Twenty-eight transmissivity data points, which are nearly uniformly distributed in the pit, were used for the geostatistical study (Fig. 5c). In this study, the transmissivity data from the pumping tests

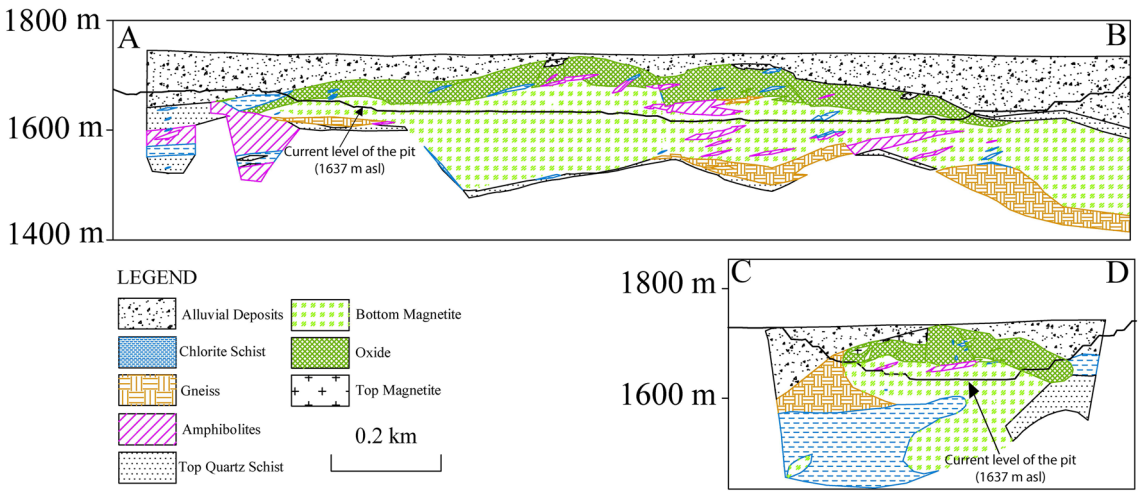

Fig. 3 Cross section along the AB and CD line in Fig. 2. The main lithology is bottom magnetite (Kusha Maadan Consulting Engineers 2006)

Table 1 The average hydrogeological and hydrochemical properties of the two major aquifers in the study area

	Bottom elevation (m asl)	GWL (m asl)	EC (mS/cm)	Transmissivity (m^2/d)
Upper aquifer (alluvium)	1546–1687	1685.11	10.84	188.9
Lower aquifer (hard rock)	–	1681.87	24.13	299.4

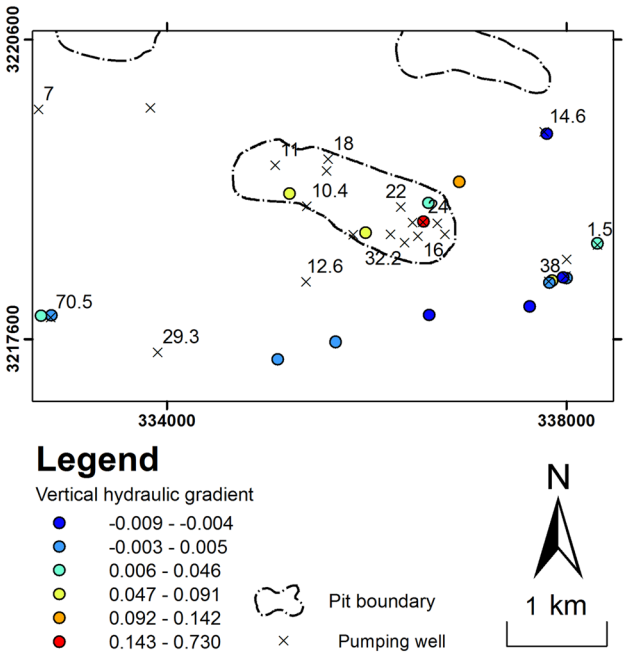

Fig. 4 Vertical hydraulic gradient for different parts of the study area. These gradients were calculated from the hydraulic heads in the piezometers installed at different depths of the aquifer. The vertical hydraulic gradient increased towards the pit, where there were more pumping wells. Positive values show downward leakage from the upper aquifer into the lower aquifer and vice versa. The *numbers* next to the cross symbols show the discharge rate (L/s) from the pumping-wells. For a better representation of the discharge rates, refer to Fig. 2

conducted in 2006–2007 were used for the simulation of this parameter (Hosseini Sabzevari 2007). Although these data were provided for the two aquifers separately, their averages were used for the simulations.

As mentioned earlier, the lower aquifer, which has a higher transmissivity, also has higher EC values (Table 1). The 68 EC data points are shown on Fig. 5b. Two sampling campaigns were conducted during 2005–2006 and groundwater samples obtained by point samplers were analysed for hydrochemical parameters, including the EC at different depths (Oil and Water Laboratory of the Gol-Gohar Ore Mine Co). These data were averaged together to obtain a single value for each location.

As mentioned above, the lower aquifer is the main contributor of groundwater discharge from the pumping wells. High vertical gradients in the piezometers installed in the pit verify this conclusion. Groundwater levels were measured weekly in 34 observation wells from 2005 to 2012 by the Mine Drainage Division of the Gol-Gohar Ore Mine Co. These data were averaged and used in the simulation process (Fig. 5a).

During mine development, thousands of blast holes were drilled to excavate or remove rock using bulk industrial explosive mixtures. They ranged in depth from 1.3 to 60 m. The 41,810 blast holes in the study area were distributed among the 10 benches of the Gol-Gohar open-pit mine (Table 2), with elevations ranging from 1687 to 1637 m asl. The groundwater level was measured in each blast hole before the explosions from 1992 to 2012. Groundwater levels recorded in the blast holes were not used in the simulation process, but were instead used to show the increased effects of fracture zones with depth.

Exploratory-Spatial Data Analysis (ESDA)

Exploratory data analysis to become familiar with the general properties of variables is a prerequisite to any geostatistical study, before applying any estimation or simulation method. Exploratory data analysis includes the examination of data maps, histograms, and variograms. Histograms were used to evaluate the statistical parameters of the desired variables. Curves were also fitted to the histograms of each variable to remove observed fluctuations. This process increases class resolution and extends the distribution beyond the minimum and maximum values. Finally, the smoothed histograms were used as an objective function in the simulated annealing algorithm. The program histsmth, implemented in the WinGSLIB software (Deutsch and Journel 1998), was used to smooth the histograms.

Variograms are representative of the spatial continuity of variables in space, and can be used to deduce the pattern of variability with distance. The semi-variogram value, $\gamma(\mathbf{h})$, can be computed using the following relation (Isaaks and Srivastava 1989):

$$\gamma(h) = \frac{1}{2N(h)} \sum_{(i,j)|h_{ij}=h} (v_i - v_j)^2 \quad (1)$$

where **h** represents the distance vector, and N(**h**) is the number of data points separated by **h** vector and corresponding values of v_i and v_j. Like the histogram, this measure also shows fluctuations, based on the number of pairs

used for computing the γ(**h**) values. Thus, it is imperative to fit a model to the experimental variogram. Basic models, such as the spherical, Gaussian, exponential, and power functions are used for this purpose. Three major parameters, the nugget, sill, and range, should be defined for each model. The nugget parameter defines the behaviour of variables at very small distances. If this parameter is high, it means that the variable of interest varies widely, even at small scales. The sill is usually equivalent to the population variance, but in some cases it may be higher. The range parameter shows at which distance the dependency of variables disappears. There are two approaches for fitting the basic models to the experimental variograms. The first is automatic fitting, which uses criteria such as the R^2 value and the residual sum of squares (RSS) to determine the quality of the fitted model to the experimental variogram, wherein the modeller does not have a role in this process. The other approach uses the judgment of the modeller to define parameters such as the sill, nugget and range for the selected basic models. The latter approach is more appropriate than the preceding one in that it can consider the nature of the desired variables (Goovaerts 1997). In this study, the visual modelling approach was used to fit the basic models into the experimental variograms. The RSS criteria was also computed to judge the quality of the fitted models.

Simulated Annealing

Simulated annealing was used to simulate the hydrogeological and hydrochemical variables. Stochastic simulations have several advantages over estimation methods such as kriging. They can be used to create several equiprobable realizations of the variable, each providing an alternative

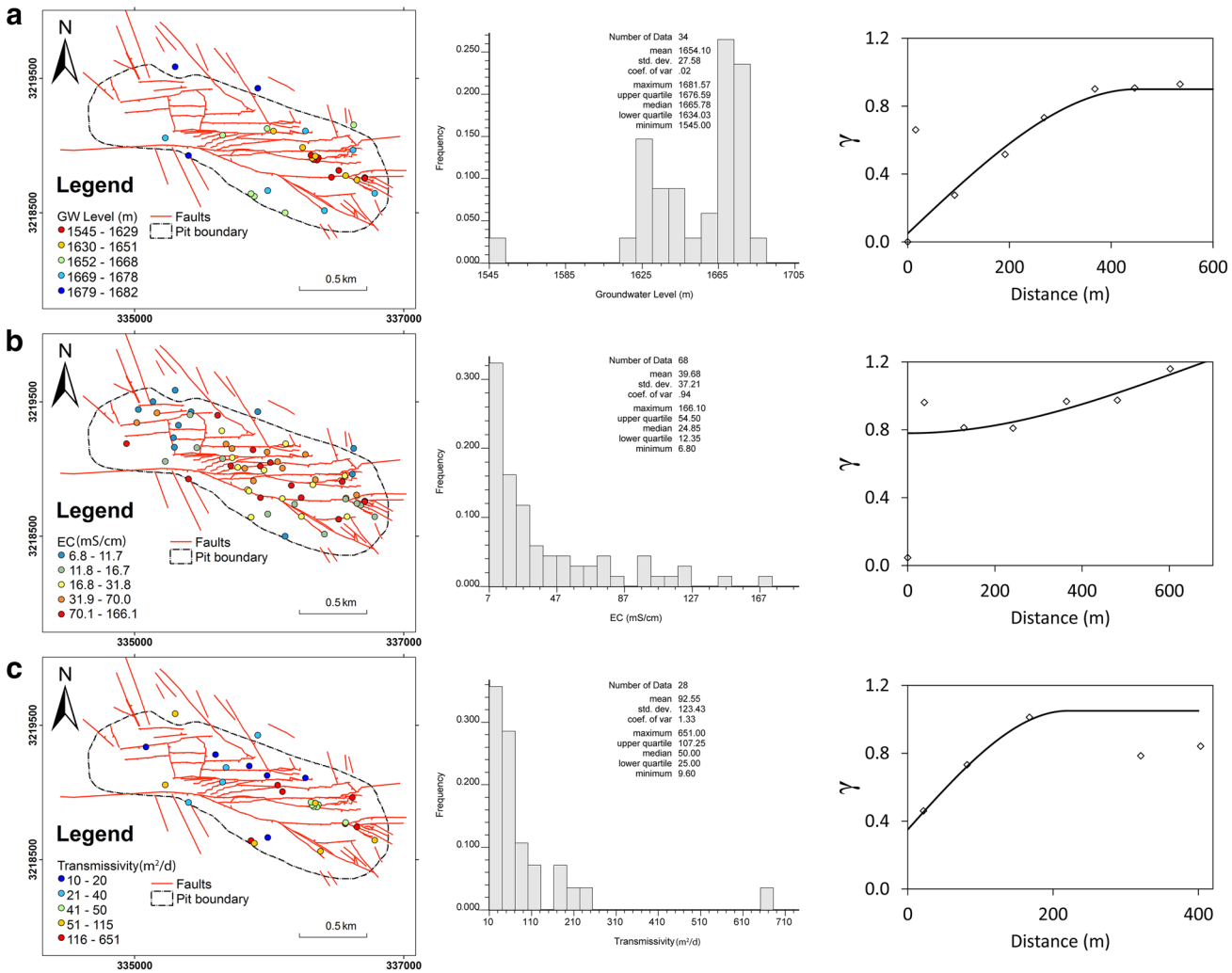

Fig. 5 The location maps, histograms, and omnidirectional variograms for: **a** the groundwater level (m asl); **b** the electrical conductivity (mS/cm); and **c** the transmissivity (m^2/day)

representation of the unknown true map, whereas in estimation methods only one prediction is obtained for each location (Remy et al. 2009). This makes them very useful tools for quantifying the uncertainty of variables. Also, the non-normality of variables is not a concern in some methods, such as the simulated annealing, since it has the capability to simulate variables with high-low skewness. This has the advantage to be customized with several objective functions, the most common of which are the histogram, data conditioning, variogram, conditional distribution and correlation with a second variable. A weakness of the simulated annealing approach is that if only two-point statistics, i.e. variograms, are considered in the simulation process, the final results will not represent the connectivity of the extreme values being observed in heterogeneous media. In these cases, the multiple-point statistics (MPS) algorithm is a better option (Strebelle 2002). In our study, this was not a critical problem because the final results were not used in a numerical groundwater flow model.

Therefore, the simulated annealing algorithm was used to simulate the groundwater level, EC, and transmissivity. In this study, three objective functions, data conditioning, histogram, and variogram, were used for this purpose. Data conditioning means that the data values are honoured at the measurement locations. This is simply achieved by fixing the cell values and disallowing any perturbation during the simulation (Deutsch and Journel 1998). The statistical histogram parameters are another important condition that should be reproduced in the final simulation. This constraint is simply achieved by assigning a random value at each grid node by drawing from the cumulative distribution function (cdf). The only remaining condition is the variogram, which contains information about the spatial continuity of the variables. This objective function is more important than the data conditioning and histogram since it can totally change the final results. During the simulation process, the grid node values are perturbed and the experimental variogram is computed for each perturbation. If the difference between the variogram of the realization and a model variogram, which is defined as an objective function, is decreased, the perturbations are accepted. This can be stated as the following relation (Deutsch and Journel 1998):

$$O = \sum_{h} \frac{[\gamma^*(h) - \gamma(h)]^2}{\gamma(h)^2} \quad (2)$$

where $\gamma(\mathbf{h})$ is the fitted model to the experimental variogram (objective function) and $\gamma^*(h)$ is the experimental variogram for each perturbation calculated from the simulated realization. O is the objective function for the variogram.

Simulated annealing was performed following these steps (Goovaerts 1997):

(1) A random image which honours data values at their locations was produced. This image must have a frequency distribution similar to the target histogram.
(2) A variogram was computed for this image, $\gamma^*(h)$, and then compared with the target variogram, $\gamma(\mathbf{h})$. The difference between these variograms is a measure of the similarity between the spatial continuity of the variable and the simulated image.
(3) The image was perturbed using a random mechanism and again the difference between the modeled variogram and target variogram was computed, O_{new}. If the difference is less than what is computed in the preceding step, i.e. $O_{new} < O$, the changes are accepted.
(4) If the perturbation was accepted, the initial realization was updated with the objective function of $O = O_{new}$.
(5) Steps 3 and 4 were repeated until the target objective function was reached.

The process can be repeated several times to create several equally probable realizations of the variable. In this

Table 2 Fitted models to the experimental variograms of different variables in the observation and blast holes and their specifications

Data			Fitted model	Range (m)	Sill	Nugget	Azimuth	Number of observations
Observation wells	GW level		Spherical	450	0.9	0.05	Omnidirectional	34
	EC		Gaussian	1600	1.78	0.78	Omnidirectional	68
	Transmissivity		Spherical	220	1.05	0.35	Omnidirectional	28
Blast holes	GW level	1687 m	Spherical	450	1.12	0.22	Omnidirectional	4127
		1675 m	Spherical	100	0.3	0.1	Omnidirectional	6235
			Exponential	550	0.65			
		1662 m	Exponential	350	1.1	0.2	Omnidirectional	4737
		1650 m	Exponential	150	1	0.1	Omnidirectional	3147
		1637 m	Exponential	70	1.05	0.2	Omnidirectional	2814

study, one hundred realizations of the desired variables were produced and their expected values (EV) computed using the following formula (Remy et al. 2009):

$$EV(z(u)) = \frac{1}{L}\sum_{l=1}^{L} z^{l}(u) \tag{3}$$

where l is the number of realization (l = 1, …, L), and $z^{l}(\mathbf{u})$ is the simulated value of z variable for the lth realization at **u** location. The geostatistical software library (GSLIB; Deutsch and Journel 1998) was used for the computation and modeling of the experimental variograms and stochastic simulations. This software contains a comprehensive collection of estimation and simulation tools that was mainly developed for mining applications but has frequently been used in other fields of science.

Multi-Criteria Decision Analysis

Multi-criteria decision analysis (MCDA) was performed on the expected values of the groundwater level, EC, and transmissivity to identify the best locations for drilling the new pumping wells. The MCDA method has been applied in various fields of study, including economy, geography, environmental studies, transportation, urban/regional planning, waste management, hydrology, agriculture, and forestry (Rinner and Voss 2013). It can be used to select the best option from a variety of choices. In GIS-based applications, the choices are the locations (coordinates), some of which are more suitable for the considered variables than other locations. Weighted linear combination (WLC) is a version of MCDA method that considers the importance of each criterion by a weight assigned to it. The WLC model has an implicit assumption that its parameters are constant over the geographical space, which is unrealistic in real-world situations. Another version of the MCDA method is the local weighted linear combination (LWLC), which assigns weights relative to the range of values observed near the considered location. This method was proposed by Malczewski (2011) and the main idea behind it is the sensitivity principle, which states that the greater the range of criterion values, the greater the weight assigned to that criterion should be. First, a range parameter, r_k^q, is calculated for the k-th criterion in the q^{th} neighbourhood (Malczewski 2011):

$$r_k^q = \max_{i,\,q}\left\{a_{ik}^q\right\} - \min_{i,\,q}\left\{a_{ik}^q\right\} \tag{4}$$

where $\max_{i,\,q}\left\{a_{ik}^q\right\}$, $\min_{i,\,q}\left\{a_{ik}^q\right\}$ are the maximum and minimum of the *k*th criterion for the *i*th location within the *q*th neighbourhood. Neighbourhoods can be defined in several ways, such as Rook and Queen contiguity, the distance and K-nearest neighbors (Voss 2015). After calculating the range parameter, a weight is calculated for each criterion within the *q*th neighbourhood, w_k^q, (Malczewski 2011):

$$w_k^q = \frac{\frac{w_k r_k^q}{r_k}}{\sum_{k=1}^{n}\frac{w_k r_k^q}{r_k}},\ 0 \le w_k^q \le 1 \ \text{ and } \ \sum_{k=1}^{n} w_k^q = 1 \tag{5}$$

where w_k is the global weight assigned to each criterion, i.e. the groundwater level, EC, and transmissivity. The r_k is the global range of these variables over the study area, and r_k^q was defined earlier in relation (4). Finally, the overall value for the *i*th location (LWLC result), $V\left(A_i^q\right)$, is calculated using the following formula (Malczewski 2011):

$$V\left(A_i^q\right) = \sum_{k=1}^{n} w_k^q v(a_{ik}^q) \tag{6}$$

In this relation, the $v(a_{ik}^q)$ represents the local value funcion and is calculated as follows:

$$v\left(a_{ik}^q\right) = \begin{cases} \frac{a_{ik}^q - \min\limits_{i,\,q}\left\{a_{ik}^q\right\}}{r_k^q}, & \text{for the k-th criterion to be maximized} \\ \frac{\max\limits_{i,\,q}\left\{a_{ik}^q\right\} - a_{ik}^q}{r_k^q}, & \text{for the k-th criterion to be minimized} \end{cases} \tag{7}$$

and $a(a_{ik}^q)$ represents the value of *k*th criterion for the *i*th location within the *q*th neighborhood. In this relation, the value of a_{ik}^q is standardized by the range variation of the considered criterion, r_k^q, within the corresponding neighbourhood.

The only parameter that should be defined is the global weights for each criterion, i.e. w_k. There are several ways to calculate this parameter, including the ranking, rating, and pairwise comparison methods (Malczewski 1999). The pairwise comparison method (Saaty 1980) was used to determine the global weights. This method is simple and well documented in the literature (e.g. Malczewski 1999). In this research, we used the "MCDA4ArcMap", an open source tool for MCDA and geo-visualization of vector data in Arc-Map. This is an ArcGIS add-in and is written in the C# programming language within the .NET environment (Rinner and Voss 2013). It has a user-friendly interface, and the main functionality contained within it is very easy to understand.

Results and Discussion

Evaluation of the Histogram and Variogram

The histogram of the groundwater level has a bimodal shape (Fig. 5a), which is attributed to the discharge from pumping wells. Several pumping wells located in the central and eastern portions of the pit have been continuously

discharging to control the invasion of groundwater into the pit. This has created a cone of depression around the pit, so that the wells located in the margin of the pit have higher groundwater levels than the wells in the central part of the pit. The mean groundwater level is 1654.1 m asl; the minimum and maximum levels were 1545.0 and 1681.6 m asl, respectively. A spherical model was fitted to the experimental variogram with a range and nugget of 450 m and 0.05 (Tables 2, 3). The low nugget of 0.05 shows the high spatial continuity of this variable. The RSS value for the fitted model is 0.057 and it shows that the visual fitting procedure worked well. This model was used as an objective function during the simulated annealing simulation (Relation 2). Because the number of data points for this variable is limited (34), it is impossible to evaluate its variogram in different directions. Instead, the groundwater level in the blast holes were used to accomplish this task. Since these wells are closely spaced, they provide an opportunity for detailed study of their variograms and spatial continuity.

Figure 6 shows the directional variograms for the 45° and 135° azimuth. In the 135° azimuth direction, the variogram has a continuous monotonically increasing trend, but in the 45° azimuth direction, the $\gamma(\mathbf{h})$ values were reduced at a distance of 400 m. This shows that the groundwater level was more continuous in the 135° azimuth direction than in the 45° azimuth direction. This may be due to the fact that the faults have a NW-SE trend, and control the groundwater distribution within the pit. This conclusion was verified later by the EC variogram. The reduction of $\gamma(\mathbf{h})$ in the 45°azimuth direction is called a hole effect and is observed in situations where there is some cyclicity with distance in the variables. Such cyclicities may reflect the orientation of faults. Chihi et al. (2013) used geostatistical modelling to examine reservoir-architecture models of a structurally complex geologic setting in the Jeffara Basin (South East Tunisia); they used variograms as the main tool to measure the spatial variability of the studied geologic medium before making any estimation or simulation. They found that the hole effect accurately expressed the cyclicity of the fault effect on the surface.

Figure 5b shows the location of the EC data points, which were uniformly distributed in the pit. The EC has a positively skew distribution with a mean of 39.673 mS/cm and a wide variation range; the coefficient of variation was 0.94. Variograms of this variable did not show any interpretable structure; therefore, their values were transformed to logarithms, and the variogram was computed again. These results are shown in Fig. 5b and Table 2. A Gaussian model with a range of 1600 m and nugget of 0.78 was fitted to the experimental variogram (Table 3). The fitted model has a value of 0.101 for the RSS criteria. Although the RSS criteria has a larger value than the groundwater level, it should be noted that the first point in the experimental variogram has a large effect on the RSS. The $\gamma(\mathbf{h})$ value for this point was calculated using only 36 data pairs, and thus it is unwise to consider it in the fitting procedure. The high nugget value, 0.78, for the EC variable means that it has a low spatial continuity. Also, the high sill of the variogram (1.78) indicates that the EC was not stationary over the study area. This conclusion was verified by the increasing trend of EC values toward the centre of the pit. Directional variograms for the 45° and 135° azimuths are shown in Fig. 7. It is evident that the variogram does not show any trend along the 45° azimuth, but the trend in the 135° azimuth shows the increasing tendency of $\gamma(\mathbf{h})$ with distance. As stated earlier, this difference with azimuth direction may be attributed to the fact that the faults have a NW-SE trend, which controls groundwater movement.

Figure 5c shows the spatial distribution of the transmissivity data. High values of this parameter are

Table 3 Fitted models to the experimental variograms and their corresponding RSS criteria

GW level	$\gamma = 0.05 + 2.8333 \times 10^{-3}\, h - 4.6639 \times 10^{-9}\, h^3$	0.057
EC	$\gamma = .078 + [1 - exp\ (1.1719 \times 10^{-6}\, h^2)]$	0.101
Transmissivity	$\gamma = 0.35 + 4.7727 \times 10^{-3}\, h\ 3.2870 \times 10^{-8}\, h^3$	0.148
1687 m	$\gamma = 0.22 + 3.0000 \times 10^{-3} h - 4.9383 \times 10^{-9} h^3$	0.240
1675 m	$\gamma = 0.75 + 4.5000 \times 10^{-3}\, h - 1.5000 \times 10^{-7}\, h^3 - 0.65 \exp(-5.4545 \times 10^{-3}\, h)$	0.111
1662 m	$\gamma = 1.1 - 0.9\ exp\ (-8.5714 \times 10^{-3}\, h)$	0.375
1650 m	$\gamma = 1.0 - 0.9\ exp\ (-2.0000 \times 10^{-2}\, h)$	0.018
1637 m	$\gamma = 1.05 - 0.85\ exp\ (-4.2857 \times 10^{-2}\, h)$	0.047

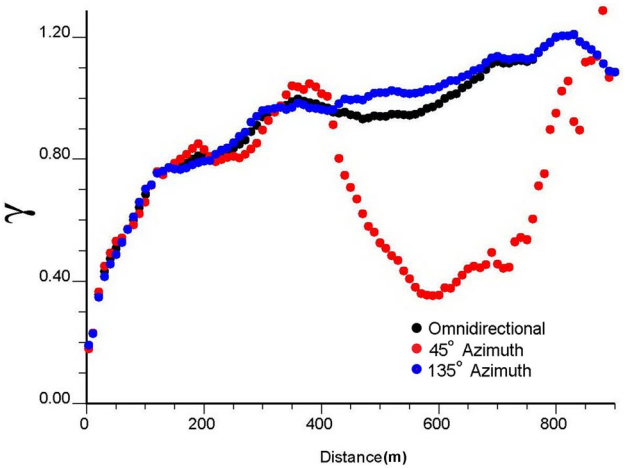

Fig. 6 Directional and omnidirectional variograms of the groundwater level in the blast holes. The omnidirectional variogram is illustrated with *black dots*. Directional variograms for the 45° and 135° azimuth are illustrated with *red* and *blue* points, respectively

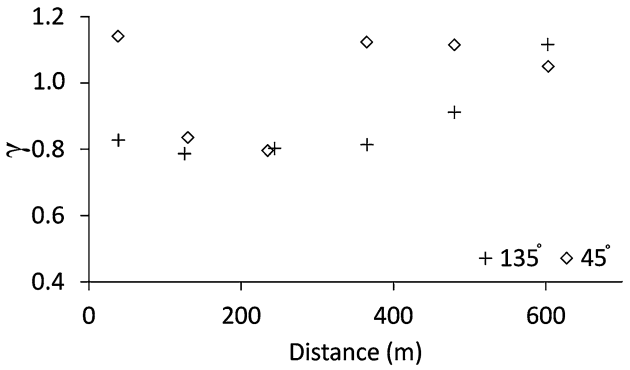

Fig. 7 Directional variograms for the electrical conductivity. There is no clear trend in the 45° azimuth

concentrated in the central-right part of the pit. The transmissivity also has a positively skewed distribution (Fig. 5c), with a mean and median of 92.6 and 50 m^2/day, respectively. A spherical model with a range and nugget of 220 m and 0.35 was fitted to the experimental variogram with an RSS value of 0.148 (Tables 2, 3). In this case, the two points at distances of 320 and 403 m deviate from the overall trend of the fitted model, and therefore were not considered in the fitting procedure since the structure of variograms at small distances is more important than at large distances. The number of data points for this variable is very low (28) to assess its spatial continuity in different directions. Fitted models for the experimental variograms (Table 3) were used as an objective function.

Simulated Annealing

In this section, the results of simulated annealing simulations are presented and compared to each other. Figure 8 shows the expected groundwater levels in the pit. The groundwater level decreases toward the NE of the pit. In addition, the groundwater level along the faults is lower than in the surrounding regions. As mentioned earlier, the discharge from the pumping wells and the better hydraulic

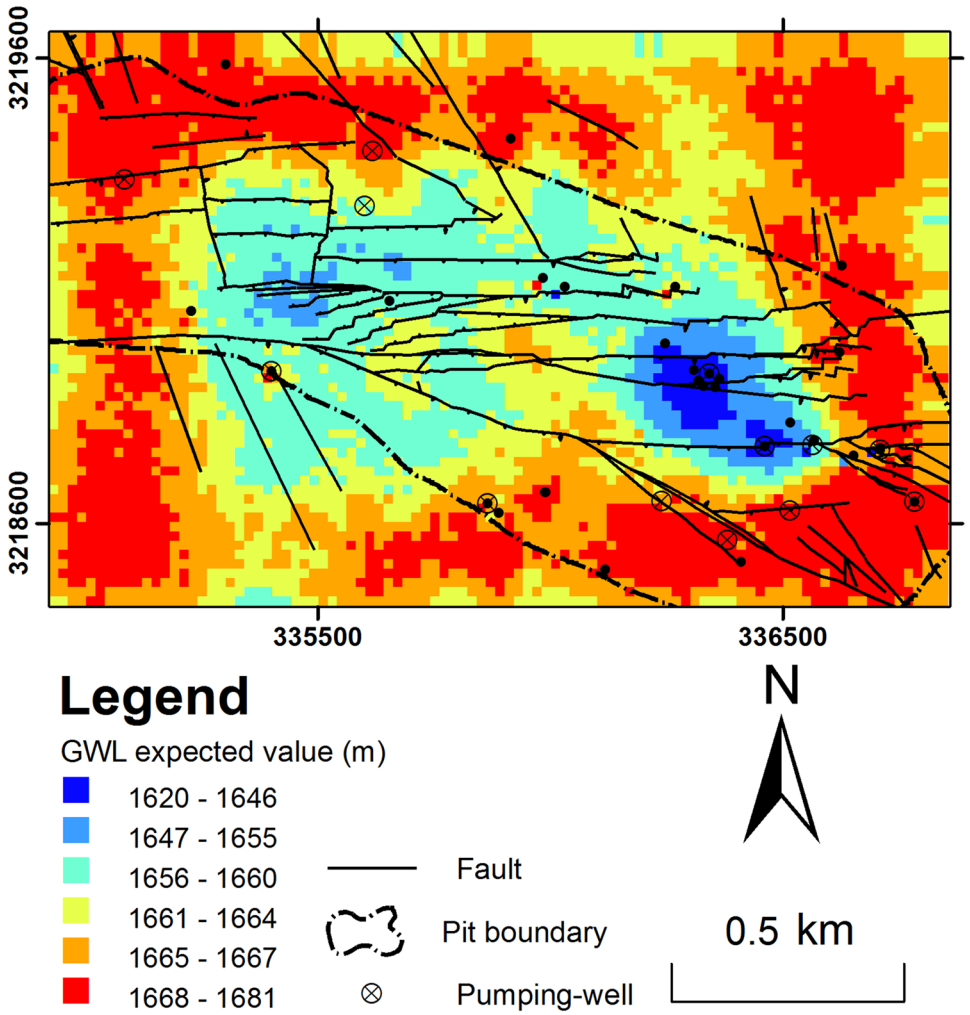

Fig. 8 Map of the estimated groundwater level (m asl) in the pit. The NE part of the pit shows the lowest values. *Black dots* show the location of data points used for the simulation of the groundwater level (Datum: WGS_1984 UTM Zone 40 N)

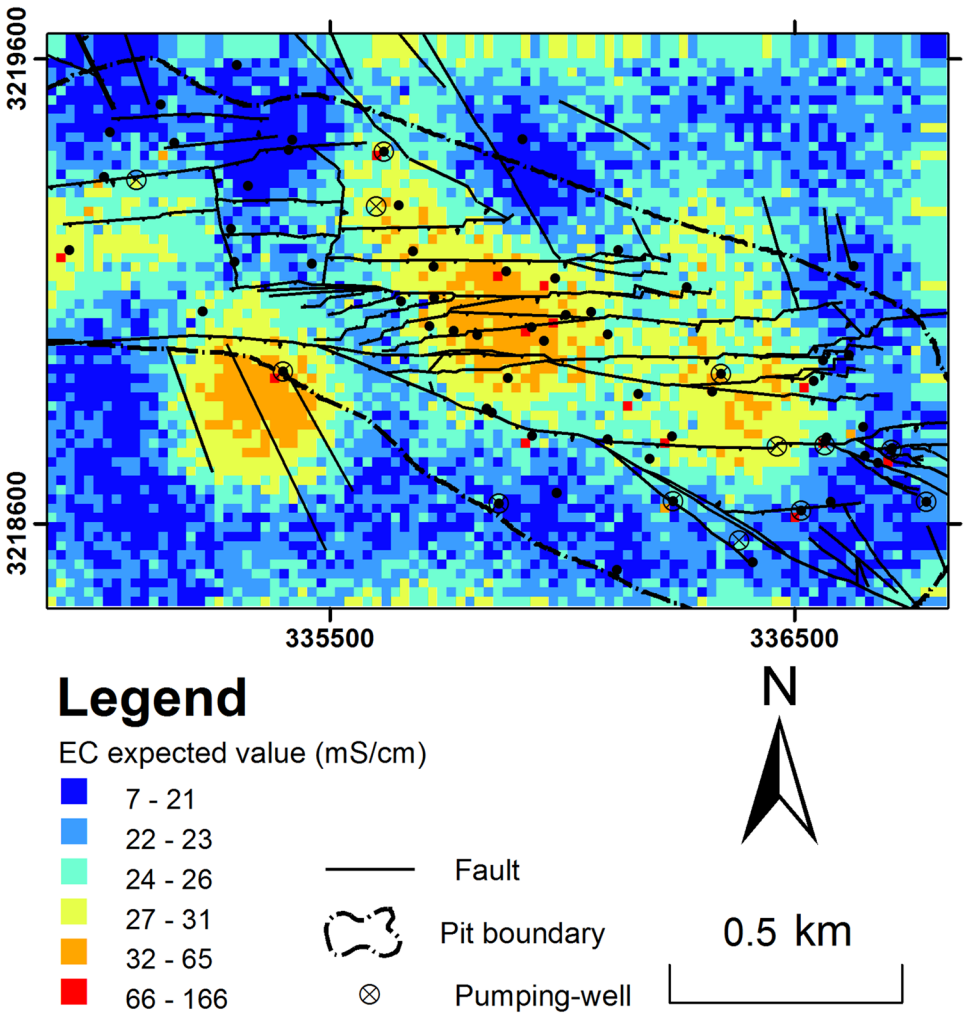

Fig. 9 Map of estimated electrical conductivity (mS/cm) in the pit. This variable shows less continuity than the groundwater level and transmissivity. *Black dots* show the location of data points used for the simulation of electrical conductivity (Datum: WGS_1984 UTM Zone 40 N)

properties of the lower aquifer are responsible for the observed cone of depression.

Expected EC values are shown in Fig. 9. The overall trend of this variable resemble that of the groundwater level. The maximum expected values exist in the central part of the pit. These simulated values show more continuity in the NW-SE direction, corresponding to the faults, rather than in the perpendicular direction. Figure 10 illustrates the expected transmissivity values. The location of the faults and high transmissivity values correlate well, and overlap, especially in the central part of the pit. Spatial distribution of this variable shows less continuity than the groundwater level (Fig. 8). This is also clear from their variograms (Fig. 5c).

There is some dependency between the expected values of the groundwater level, EC, and transmissivity. To examine this hypothesis, a scatterplot matrix, showing the interrelationship between the simulated (expected) values was produced (Fig. 11). It is evident that there is good correlation between these variables. The best correlation exists between the groundwater level and transmissivity, with a correlation coefficient (ρ) of −0.59. The *t* test of correlation showed that it is significant at the 0.01 level (2-tailed), and thus is a reliable estimate. The negative correlation is because the transmissivity increases at lower groundwater levels, i.e. the transmissivity is greater at lower depths. This agrees with our previous findings that the lower aquifer has higher transmissivity at lower groundwater levels. This conclusion is strengthened by the fact that the number and the effect of faults increase with depth. For example, the range of variograms of groundwater level in the blast holes decreases with increasing depth. Figure 12 shows these variograms for the blast holes in different benches of the pit. Table 3 shows the fitted model to the experimental variograms. The range of variograms decreased from 450 m at the 1687 m asl level of the pit to 70 m at the 1637 m asl level. This trend shows an increasing level of heterogeneity in the lower depths due to the effect of increasing fault density with depth.

Another important point about the scatterplot matrix is that the groundwater level and EC show a negative correlation, $\rho = -0.48$, with a significance level of 0.01

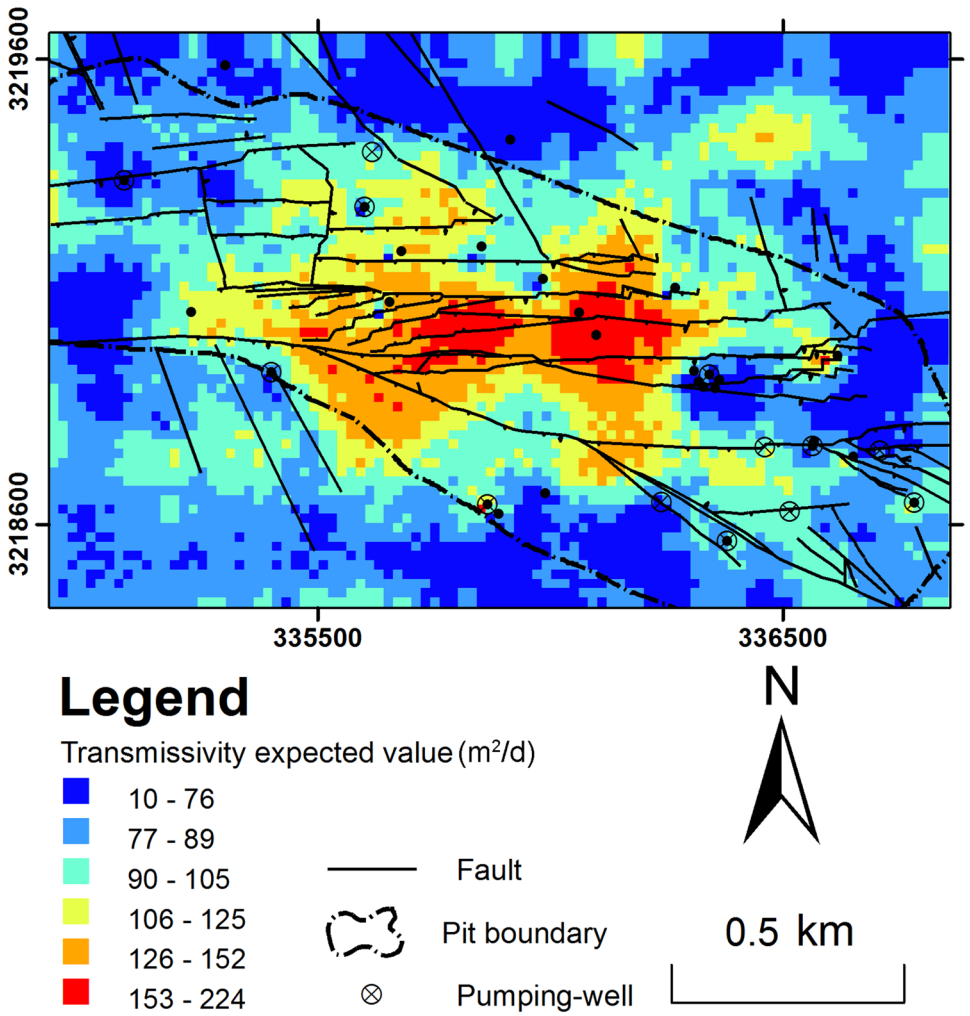

Fig. 10 Map of estimated transmissivity (m^2/day) in the pit. A good overlap exists between the location of the faults and high values of transmissivity. *Black dots* show the location of data points used for the simulation of transmissivity (Datum: WGS_1984 UTM Zone 40 N)

(Fig. 11). This relationship indicates that the groundwater quality decreases at depth. Also, there is a direct relation between transmissivity and EC with $\rho = 0.42$ (with a significance level of 0.01). As stated earlier, the increase of fault density with depth likely corresponds with the increased density of fracture zones, which causes the transmissivity of the rock to increase. The direct relation of transmissivity and EC may be attributed to the fact that the faults play a major role in the transfer of groundwater with high salinity. The saline groundwater at lower depths may originate from the Kheir-Abad salt playa in the NE part of the study area (Fig. 1), which is located 10 km from the north-eastern part of the pit. Given the high conductivity of the faults, they can easily transfer groundwater such distances. The general flow direction of groundwater is from the NE towards the SW and the depression cone of the pumping wells has created a sharp hydraulic gradient towards the central part of the pit.

The preceding discussion can be summarized as follows:

1. There is a good correlation between hydrogeological (transmissivity and groundwater level) and hydrochemical parameters (EC).
2. The direct relationship between these parameters may be due to the faults.
3. Based on the omnidirectional variograms of the blast holes, the effect of faults increases with depth.
4. The groundwater level, transmissivity, and EC spatial distributions are highly dependent on the trend of the faults.

MCDA Results

In this section, the final results of the stochastic simulations were used to define the best locations for drilling new wells. Transmissivity is the best criteria for this goal, and one can use the expected values of this variable for decision-making (Fig. 10), but as mentioned earlier, the lower groundwater level and higher EC values also indicate that the hard rock aquifer has better hydraulic properties. To determine the global weight of these parameters (w_k) in the

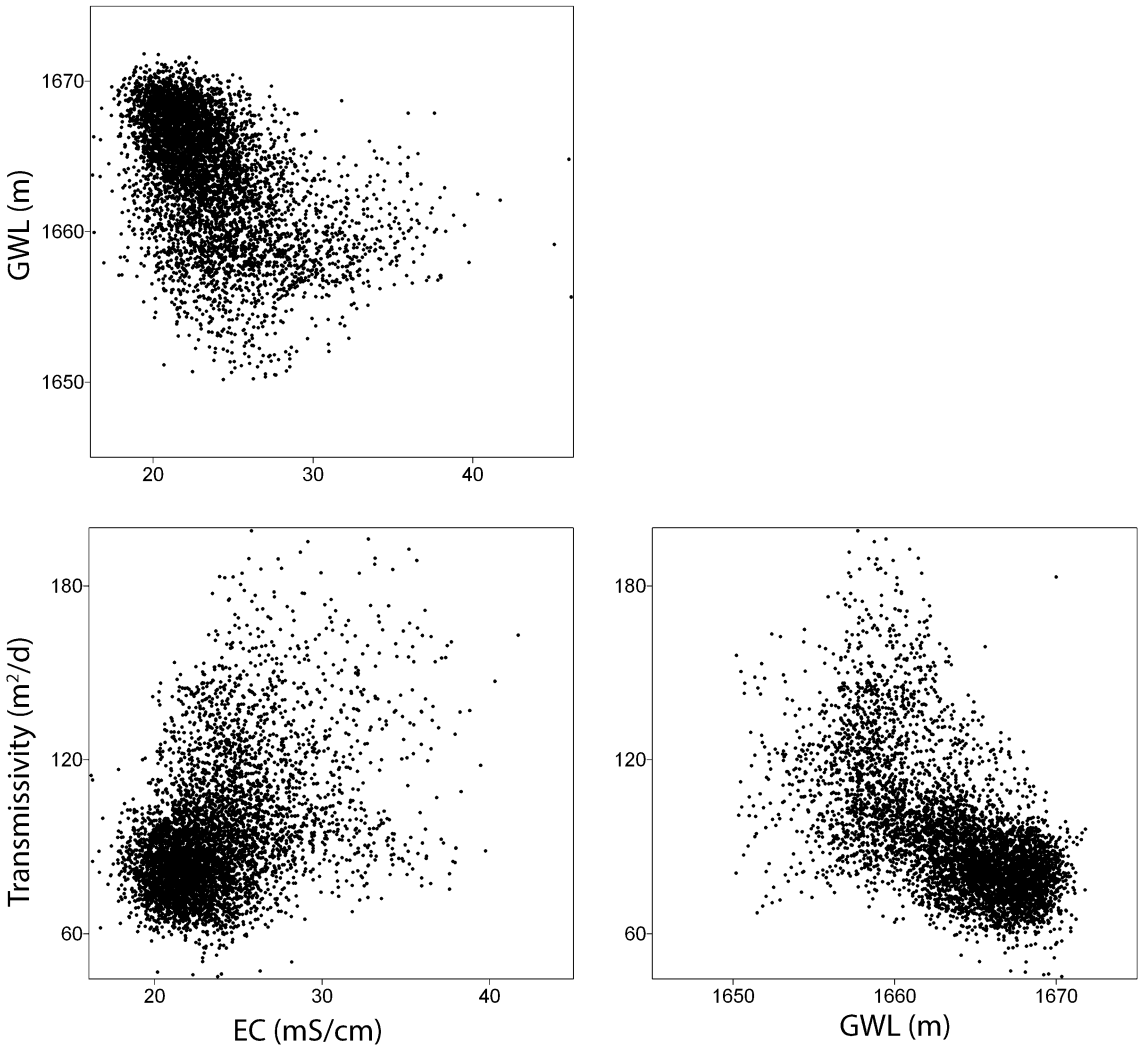

Fig. 11 The scatterplot matrix showing the relationship between pairs of expected values of the groundwater level, EC, and transmissivity

MCDA method, the pairwise comparison method developed by Saaty (1980) was used. First, a ratio matrix reflecting the importance of each criterion relative to the others was created (Table 4). A value of 7 (very strong importance) was assigned to the transmissivity criteria against the groundwater level. This is because the transmissivity is very important in defining the best location for drilling new wells against the groundwater level. A value of 6 (strong to very strong importance) was selected for the transmissivity against the EC. The groundwater level is less important than the EC criteria because it has less of a variation range (3.24 m) than the EC parameter (13.29 mS/cm). Therefore, a value of 3 (moderate importance) was assigned to the EC criterion relative to the groundwater level. Other elements of the ratio matrix were achieved by the reciprocal of the preceding values, i.e. 1/7, 1/6, and 1/3. In the next step, the sum of each column of matrix was calculated and then each element was divided into its column total to obtain the normalized pairwise comparison matrix. Finally, the sum of normalized scores for each row was divided by 3 to obtain the global weight for each criterion. These weights include: the transmissivity: 74.13%; EC: 17.74%; and groundwater level: 8.13%. The consistency ratio (CR) showed that the obtained weights were consistent; if the CR ratio exceeds 0.1, the elements of the ratio matrix are not correctly defined and should be revised (Saaty 1980). For our ratio matrix, this parameter was calculated to be 0.07, which is obviously less than 0.1.

The computed global weights were used in the LWLC method to calculate the the overall value for the *i*th location, i.e. $V\left(A_i^q\right)$, from the available alternatives. The final results of the simulations, i.e. the three maps of expected values, were imported into the ArcGIS environment and the MCDA4ArcMap add-in was used to select the criteria and assign their corresponding global weights. Also a threshold distance of 40 m was selected to define the

neighnourhoods for which the range parameter, r_k^q, would be calculated. Considering the threshold distance definition, 13 grids (blocks) were selected around the *i*th location to define the neighbourhoods for the calculation of the range parameter. The transmissivity and EC criterias were defined as a "Benefit" in the MCDA4ArcMap add-in. This means that the greater the values of these parameters are, the higher the weights that should be assigned to them. Finally, the model was run to combine the layers with assigned weights.

Figure 13 demonstrates the best locations proposed for boring new wells. These locations were selected based on the overall value for the *i*th location, $V\left(A_i^q\right)$, and correspond with the highest values obtained for $V\left(A_i^q\right)$. A good overlap exists between the proposed locations and the faults, with some exceptions in the northeastern and southern parts of the pit. However, there is a small overlap between the proposed sites and pumping well locations. This may be due to the fact that the current location of pumping-wells was not optimized from the hydrogeological point of view, and there may be potential locations (proposed sites) that have better hydraulic parameters than the current pumping well positions. The proposed locations can be used to define places with higher hydraulic properties, which is desirable for efficient draining operations.

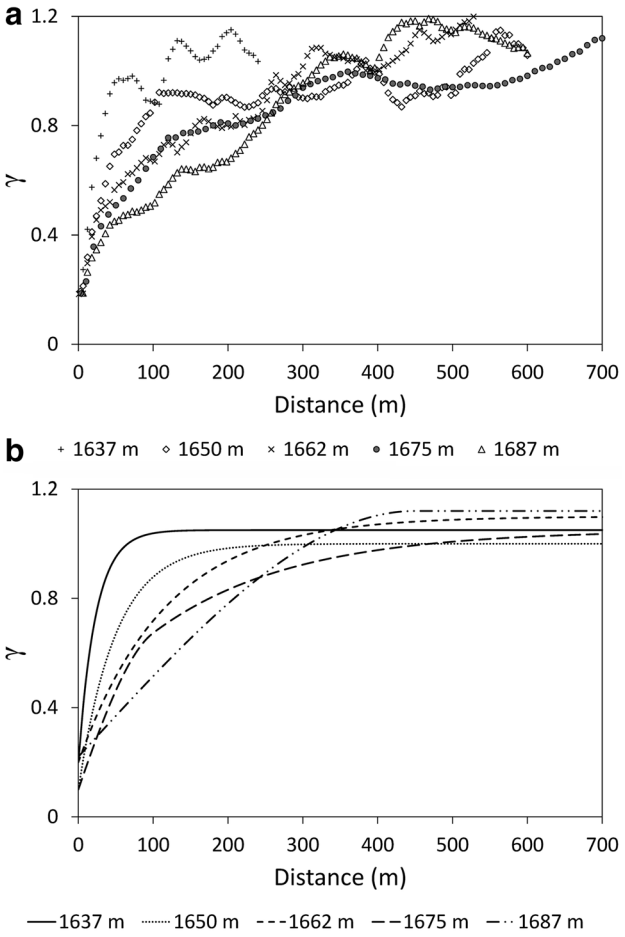

Fig. 12 Omnidirectional variograms of the groundwater level in the blast holes for several of the pit benches. Notice the decreasing trend of the variogram range with depth

Conclusion

The groundwater level, EC, and transmissivity were analysed and simulated by the use of geostatistical stochastic simulations, and then combined together using the MCDA method to find the best locations for drilling new pumping wells. A simulated annealing simulation was performed on these variables to obtain a view of their spatial distribution. The results showed that the faults have a major control on the spatial distribution of these variables. The groundwater level and EC spatial continuities varied with direction and showed more continuity in the NW-SE direction, similar to the orientation of faults. A relatively reliable correlation, with a significance level of 0.01, was found between the groundwater level, EC, and transmissivity in the study area. The groundwater level and EC simulated values were negatively correlated. In addition, a positive relationship was observed between the transmissivity and EC simulated values. This is believed to be due to the role of faults in the transport of saline groundwater at lower depths. Variograms of the groundwater level in the blast holes revealed that the effect of faulting intensified with depth. The faults in the upper alluvial aquifer have a minor effect on the overall spatial distribution of the groundwater level, but their effects increased with depth. These conclusions were obtained by interpreting the range of variograms. Finally, a multi-criteria decision analysis was performed on the maps of expected values to predict the best locations for drilling new wells. The approach implemented in this research can be used at other mining sites with similar hydrogeological settings to overcome uncertainties pertaining to locations for new pumping wells.

Table 4 The ratio matrix between pairs of criteria considered for MCDA method

Criterion	T	GWL	EC
T	1	7	6
GWL	0.14	1	0.33
EC	0.16	3	1
Σ	1.3	11	7.33

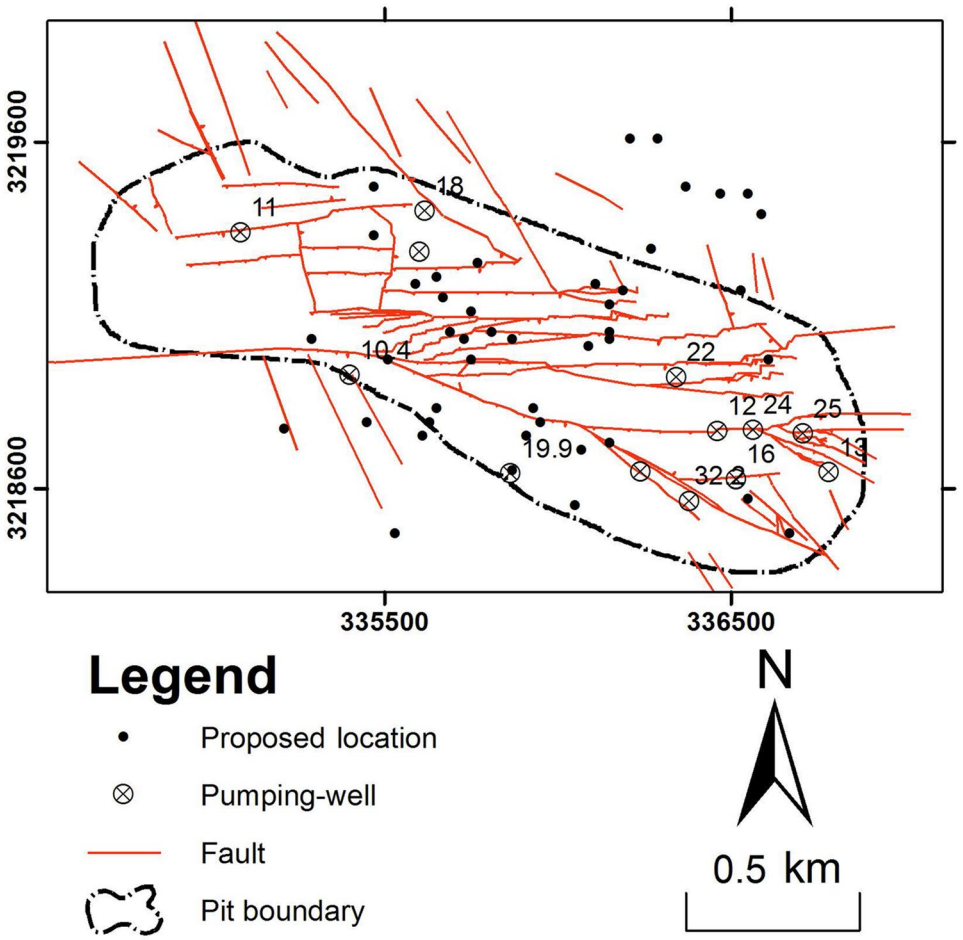

Fig. 13 Proposed locations for drilling new wells. Three measures, the groundwater level, EC, and transmissivity values, were considered in the creation of this map. The central part of the pit is the best potential location for drilling new wells. In some regions, there is an overlap between the pumping wells and proposed locations. (Datum: WGS_1984 UTM Zone 40 N)

Acknowledgements The authors thank the Gol-Gohar Mining and Industrial Company for their financial support. This research was also supported by the Research Council of Shiraz University, Iran.

References

Alavi M (1994) Tectonics of the Zagros orogenic belt of Iran: new data and interpretations. Tectonophysics 229:211–238

Bredehoeft J, Belitz K, Sharp-Hansen S (1992) The hydrodynamics of the Big Horn Basin: a study of the role of faults. AAPG Bull 76:530–546

Chandra S, Ahmed S, Ram A, Dewandel B (2008) Estimation of hard rock aquifers hydraulic conductivity from geoelectrical measurements: a theoretical development with field application. J Hydrol 357:218–227

Chihi H, Bedir M, Belayouni H (2013) Variogram identification aided by a structural framework for improved geometric modeling of faulted reservoirs: Jeffara Basin, southeastern Tunisia. Nat Resour Res 22:139–161. doi:10.1007/s11053-013-9201-0

De Marsily G, Delay F, Teles V, Schafmeister M (1998) Some current methods to represent the heterogeneity of natural media in hydrogeology. Hydrogeol J 6:115–130

Deutsch CV, Journel AG (1998) GSLIB geostatistical software library and user's guide. Oxford University Press, New York City

Forster CB, Evans JP (1991) Hydrogeology of thrust faults and crystalline thrust sheets: results of combined field and modeling studies. Geophys Res Lett 18:979

Golestanifar M, Ahangari K (2012) Choosing an optimal groundwater lowering technique for open pit mines. Mine Water Environ 31:192–198

Goovaerts P (1997) Geostatistics for natural resources evaluation. Oxford University Press, New York City

Hill MC, Tiedeman CR (2006) Effective groundwater model calibration: with analysis of data, sensitivities, predictions, and uncertainty. Wiley, New York

Hosseini Sabzevari M (2007) Evaluating the hydrogeological characteristics of aquifer in the Gol-Gohar mine, Sirjan. Shahrood University of Technology

Huang C, Mayer AS (1997) Pump-and-treat optimization using well locations and pumping rates as decision variables. Water Resour Res 33:1001–1012

Huysmans M, Dassargues A (2009) Application of multiple-point geostatistics on modelling groundwater flow and transport in a cross-bedded aquifer (Belgium). Hydrogeol J 17:1901–1911

Isaaks EH, Srivastava RM (1989) An introduction to applied geostatistics. Oxford University Press, New York City

Jang CS, Liu CW (2004) Geostatistical analysis and conditional simulation for estimating the spatial variability of hydraulic conductivity in the Choushui River alluvial fan, Taiwan. Hydrol Process 18:1333–1350

Kusha Maadan Consulting Engineers (2006) The five-year management report of the Gol-Gohar Mine (Status Map)

Kusha Maadan Consulting Engineers (2007) Final report of hydrogeology and mathematical model of the Gol-Gohar Mine

Li L, Yang T, Liang Z, Zhu W, Tang C (2011) Numerical investigation of groundwater outbursts near faults in underground coal mines. Int J Coal Geol 85:276–288

López DL, Smith L (1995) Fluid flow in fault zones: analysis of the interplay of convective circulation and topographically driven groundwater flow. Water Resour Res 31:1489–1503

Malczewski J (1999) GIS and multicriteria decision analysis. Wiley, New York

Malczewski J (2011) Local weighted linear combination. Trans GIS 15:439–455

Morton KL, Van Mekerk F (1993) A phased approach to mine dewatering. Mine Water Environ 12:27–33

Niwas S, Tezkan B, Israil M (2011) Aquifer hydraulic conductivity estimation from surface geoelectrical measurements for Krauthausen test site, Germany. Hydrogeol J 19:307–315

Nowak W, Cirpka OA (2006) Geostatistical inference of hydraulic conductivity and dispersivities from hydraulic heads and tracer data. Water Resour Res 42(8): W08416, 6, doi:10.1029/2005WR004832

Patriarche D, Castro MC, Goovaerts P (2005) Estimating regional hydraulic conductivity fields—a comparative study of geostatistical methods. Math Geol 37:587–613

Remy N, Boucher A, Wu J (2009) Applied geostatistics with SGeMS: a user's guide. Cambridge University Press, New York City

Rinner C, Voss S (2013) MCDA4ArcMap—an open-source multi-criteria decision analysis and geovisualization tool for ArcGIS 10. Cartouche, Newslet Can Cartographic Assoc 86:12–13

Saaty TL (1980) The analytic hierarchy process: planning, priority setting, resources allocation. McGraw Hill, New York City

Smerdon BD, Turnadge C (2015) Considering the potential effect of faulting on regional-scale groundwater flow: an illustrative example from Australia's great artesian basin. Hydrogeol J 23:949–960

Soltani-Mohammadi S, Hezarkhani A (2013) A simulated annealing-based algorithm to locate additional drillholes for maximizing the realistic value of information. Nat Resour Res 22:229–237

Stevick E, Pohll G, Huntington J (2005) Locating new production wells using a probabilistic-based groundwater model. J Hydrol 303:231–246

Strebelle S (2002) Conditional simulation of complex geological structures using multiple-point statistics. Math Geol 34:1–21

Sun N-Z (1994) Inverse problems in groundwater modeling. Kluwer Academic, Dordrecht

Voss S (2015) MCDA4ArcMap. https://mcda4arcmap.codeplex.com/. Accessed 4 Feb 2015

Worthington SR (2009) Diagnostic hydrogeologic characteristics of a karst aquifer (Kentucky, USA). Hydrogeol J 17:1665–1678

Wu Q, Wang M, Wu X (2004) Investigations of groundwater bursting into coal mine seam floors from fault zones. Int J Rock Mech Min 41:557–571

Yin ZY, Brook GA (1992) The topographic approach to locating high-yield wells in crystalline rocks: does it work? Groundwater 30:96–102